Composites Part B 160 (2019) 632–643

Contents lists available at ScienceDirect

Composites Part B

journal homepage: www.elsevier.com/locate/compositesb

Fabrication of robust, ultrathin and light weight, hydrophilic, PVDF-CNT membrane composite for salt rejection

Vivek Dhand[a], Soon Kyu Hong[b], Luhe Li[b], Jong-Man Kim[a,b,c], Soo Hyung Kim[a,b,c], Kyong Yop Rhee[d], Hyung Woo Lee[a,b,c,*]

[a] Research Center of Energy Convergence Technology, Pusan National University, Busandaehak-ro 63beon-gil 2, Geumjeong-gu, Busan, 46241, Republic of Korea
[b] Department of Nano Fusion Technology, Pusan National University, Busandaehak-ro 63beon-gil 2, Geumjeong-gu, Busan, 46241, Republic of Korea
[c] Department of Nanoenergy Engineering, Pusan National University, Busandaehak-ro 63beon-gil 2, Geumjeong-gu, Busan, 46241, Republic of Korea
[d] Department of Mechanical Engineering, Kyung Hee University, Yongin, 446-701, Republic of Korea

ARTICLE INFO

Keywords:
PVDF-CNT membrane
Contact angle
XRD
FTIR
Raman
TGA
Tensile
Salt rejection

ABSTRACT

PVDF-CNT membranes were fabricated using thermally induced phase separation (TIPS) protocol. The membranes are extremely tensile, strong and robust. Membranes exhibit hydrophilic behavior with decreasing contact angle (CA $< 90^{\circ}$) in saline environment. Crystal study (XRD) of membranes reveals α-phased PVDF with hexagonal (002) oriented CNTs within the polymer matrix. The morphology (SEM) and thermal analysis (TGA) reveals that the material is made of several porous zones and the material is chemically and thermally stable up to 500 °C. Raman and FTIR spectrum shows ordered bands of the D and G with complete grafting of PVDF bonds with CNTs respectively.

1. Introduction

Poly(vinylidene fluoride) (PVDF) membrane is a boon to the scientific research where, it has been extensively applied in several industries and their process due to its superior properties [1]. PVDF is extremely stable, semi-crystalline polymer and offers higher grades of chemical resistance, thermal stability and membrane fabricating properties. Apart from these, PVDF also offers a myriad of applications which includes membrane distillation, water treatment, removal and separation of gas-pollutants, recovery of bio-energetic fuel like bio-ethanol, lithium ion battery separator and physical support for composite membrane synthesis respectively [1–5]. It is the crystalline phase of PVDF polymer which yields higher mechanical strength and resistance towards impacts, wear and tear, whilst the amorphous phase renders flexibility to the membrane [6]. PVDF is easy to dissolve in several organic solvents like N-methyl-2-pyrrolidone (NMP), N,N-dimethylformamide (DMF), N,N-dimethylacetamide (DMAc), acetone and Tetrahydrofuran (THF) etc., which helps in fabrication of porous membranes by several methods involving simple phase inversion protocols. These protocols are the most common industrial procedures employed to yield out large scale production of membranes [1,6]. Since PVDF is highly compatible with process-ability, it can be synthesized in forms like flat sheet, rolls or bands of hollow fiber and tubular membranes.

Hydrophobicity/philicity is an important parameter for any PVDF membrane, as several commercial membranes are made of PVDF as its primary component. The efficiency and performance of PVDF membrane depends on the degree of resistance produced against fouling and wetting process, which consequently maximizes the operation cost and failures. Hence the PVDF membranes are modified accordingly to either make it hydrophobic/phillic to provide effective, improved anti-fouling and wetting resistance [7,8]. This area has specially gained a lot of attraction and has opened research with myriad possibilities in the field of membrane filtration. In addition, the comparatively high mechanical robustness of PVDF offers advantage over other materials in fabrication of membranes useful for water treatment processes [6]. Based on these traits of PVDF, if a 1D filler is added within its matrix it would result in synergistic advantage of properties there by making the membrane more robust, lightweight, with improved hydrophobicity/phillicity and chemical stability. Such 1D filler is a carbon nanomaterial (CNM) in the

Abbreviations: PVDF, Poly (vinylidene fluoride); TIPS, Thermally Induced Phase Separation; CA, Contact angle; CNT, Carbon nanotubes; XRD, X-ray diffraction; SEM, Scanning electron microscope; TGA, Thermogravimetric analysis; FTIR, Fourier transform infrared spectroscopy

* Corresponding author. Department of Nanoenergy Engineering, Pusan National University, Busandaehak-ro 63beon-gil 2, Geumjeong-gu, Busan, 46241, Republic of Korea

E-mail address: LHW2010@pusan.ac.kr (H.W. Lee).

https://doi.org/10.1016/j.compositesb.2018.12.106
Received 25 September 2018; Received in revised form 18 December 2018; Accepted 26 December 2018
Available online 28 December 2018
1359-8368/

form of carbon nanotubes (CNTs) which will offer more promising results in the membrane technology [9–13]. Generally the combinatorial mix of 1D Carbon nanomaterial (viz. CNTs) with polymers offers the combined merits of organic-inorganic, physico-chemical interactions and synergistic enhancement in electrical, thermo-mechanical, filtration/separation properties respectively [9,14,15].

The primary objective of the present work is to assess the ability of water passage through an ultra thin composite membrane of the VACNT forest and the PVDF. Where the saline water should be able to have a free passage through the matrix for desalination application. Thereby, maintaining its hydrophilic nature so as to avoid any possible fouling. Authors would like to emphasize that the present work is to fabricate an ultra thin membrane within the norm of 100 μm using the TIPS method. So that the energy efficiency and higher water flux for the system working at low pressure (1bar) is achieved. More over the composite is designed in such a way using thermal (TIPS) approach so that the thickness of the composite is well maintained below 100 μm (our case max thickness = 60 μm) with very high mechanical strength. Based on these findings the novelty of the work is the use of TIPS protocol to create a VACNT-PVDF based membranes for active desalination. Moreover it is a known fact that most of the desalination membranes are made of PVDF, Polypropylene or PVA based polymers as their master matrix for various support fillers. It is the functional and molecular aspect of these composites which attributes to its novelty and efficiency.

Hence, the present work describes the fabrication of PVDF-CNT membrane composite with higher mechanical robustness and improved hydrophilicity of the membrane synthesized by blending and TIPS method.

2. Experimental techniques

2.1. CNT synthesis

Synthesis of vertically aligned (VA) CNTs were carried out at first by depositing the catalysts iron (Fe) and alumina (Al_2O_3) on single crystal (100) Si Wafer (p-type, boron doped; Winwin Tech; Korea) by an electron beam evaporator (Samhan thin film vacuum Co. Ltd., Korea). The deposited Alumina also acts as a porous substrate and a thin film buffer layer for enhancing the growth of CNTs [16–19]. The Fe—Al_2O_3 catalyst coated Si wafer is then transferred to a CVD (ISAC Research, Inc. Korea) chamber made of quartz tube equipped with furnace and a quartz seat respectively. Fig. 1 shows the in-house developed CVD system scheme for VACNT synthesis. In this system the CNTs are synthesized by slowly pre-heating the furnace up to 520 °C at a ramp rate of 20 °C/min in the presence of argon (Ar) and Hydrogen (H_2) gas respectively. At this temperature, the pre-treatment process makes the catalyst transform itself in the form of nano-phased “catalytic islands” [20,21] on the Si wafer. This process not only helps in obtaining high quality CNTs, but also synthesizes uniform diametric CNTs. After this step, the synthesis of CNTs occur with the release of both H_2 and acetylene (C_2H_2) gas in a 4:1 ratio for 30 min when the temperature reaches 700 °C.

2.1.1. Catalyst deposition

Before the synthesis of CNT, catalyst is prepared by depositing Fe and Al_2O_3 on a clean silicon and a silicon dioxide (Si) wafer using an electron beam evaporator. We deposit 20 nm thick buffering layer of alumina followed by a 2 nm thick iron catalyst on top at a deposition rate of 0.3–0.4 Å, under a high vacuum pressure of 10^{-4} torr respectively. In general, during the process a gaseous state of atomized catalyst is formed which gets condensed and deposited as a thin film on the wafer uniformly due to a temperature based gradient within the chamber. Using a system in-built detector, the thickness is monitored in real time during the deposition process. On completion, the coated wafer with catalyst is transferred to the CVD system for CNT synthesis. Fig. 2(a) depicts the catalyst deposition layout for the synthesis of CNT along with the CVD ramping procedure Fig. 2(b).

2.2. PVDF-CNT composite fabrication

PVDF-CNT membranes are fabricated through temperature induced phase separation technique (TIPS) with a modified procedure [15] as depicted in Fig. 3. The casting solution is prepared by mixing (in weight/weight percentage = w/w%) the required amount of PVDF 10%, 15%, and 20% (Alfa Aeser (44080: $(-CH2CF2-)_n$ MP:155–160 °C), Korea) and 90 w/w %, 85% and 80% of *N*-methy-2-pyrrolidone (NMP, Sigma-Aldrich, Korea) at 70 °C until mixed and vigorously stirred using stirrer at maximum RPM. After complete dissolution of the PVDF in the NMP, the solution is degassed under vacuum for removal of any air bubbles.

Then the composite membrane is fabricated by casting the liquid

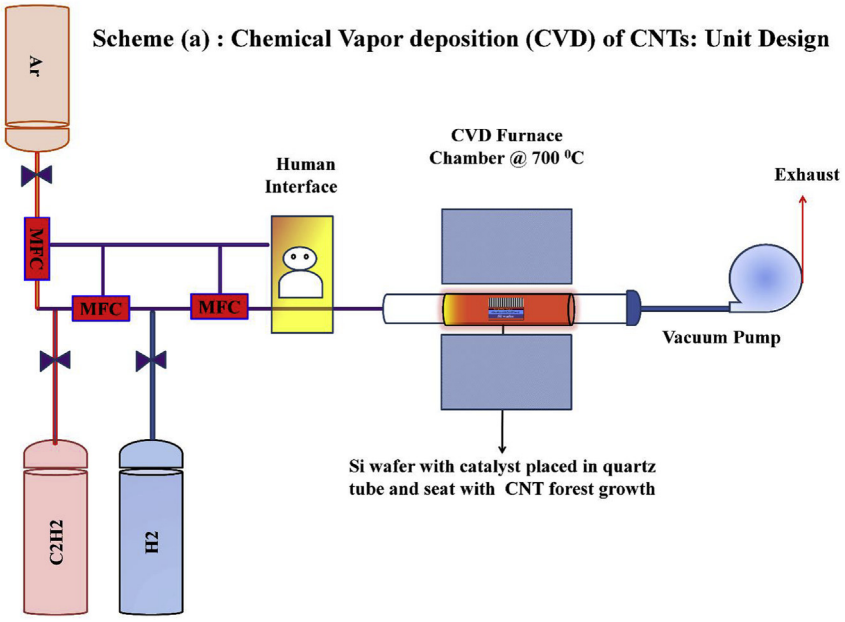

Fig. 1. Synthesis of CNTs using CVD and its unit design scheme.

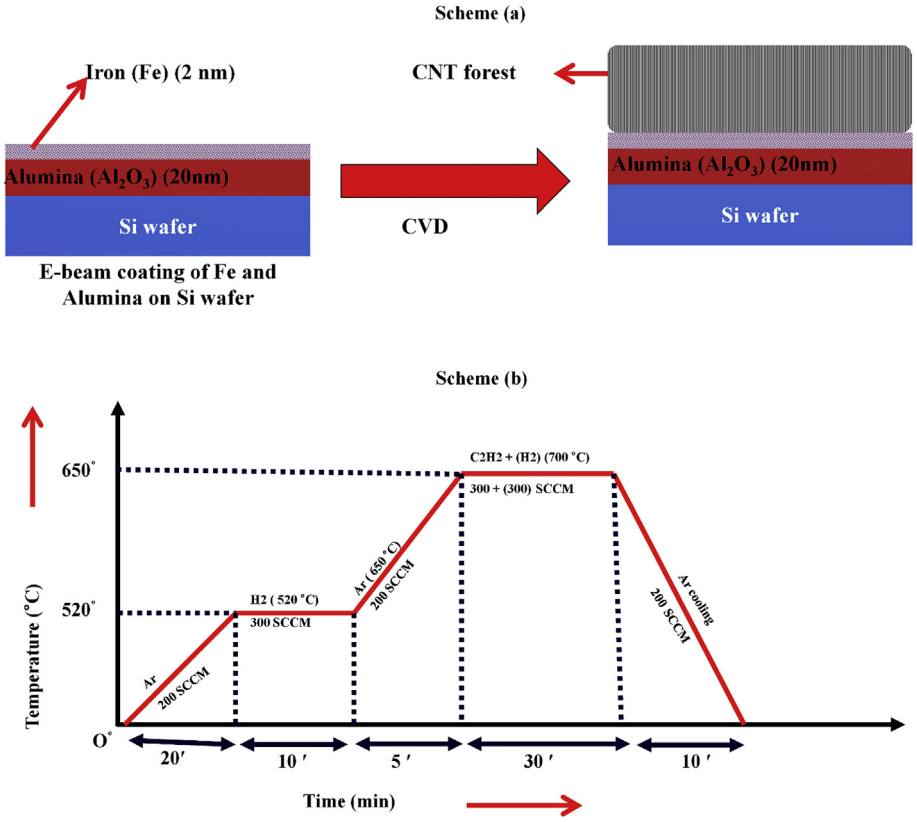

Fig. 2. Scheme (a): E-beam based catalyst (Fe and Alumina) coating on Si wafer for synthesis of CNT forest. Scheme (b): Temperature program parameters and the ramp rate of the CVD equipment for the CNT synthesis.

solution on to the CNT synthesized Si wafer at room temperature. Once the wafer is completely covered by the thin layer of the PVDF solution, it is allowed to dry in the air for 15 min and then kept on a hotplate controlled at 55 °C for 12 h. Once the film is dried it can be pulled out easily (Step.1). If it doesn't pull out, then the wafer with CNT-PVDF film is immersed in a 50 ml of 1:3 ratio HNO_3: HCl to remove the CNT holding from the Fe catalyst. This causes the complete detachment of CNTs from wafer and the membrane is now free-standing (Step.2). The

Table 1
PVDF, PVDF-CNT membrane recipe.

EXPT NO	PVDF (g)	CNT (g)	NMP Solvent (g)	w/w %
Pure PVDF	0.75	0	15	5%
PVDF10%—CNT	1.5	0.01	15	10%
PVDF15%—CNT	2.25	0.01	15	15%
PVDF20%—CNT	3	0.01	15	20%

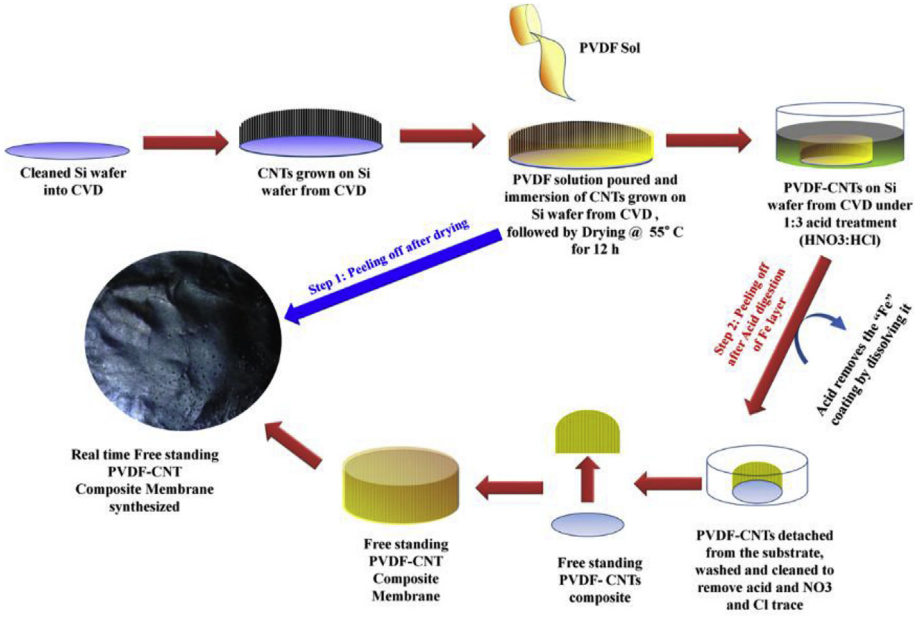

Fig. 3. Step wise procedure for the synthesis of PVDF-CNT membranes.

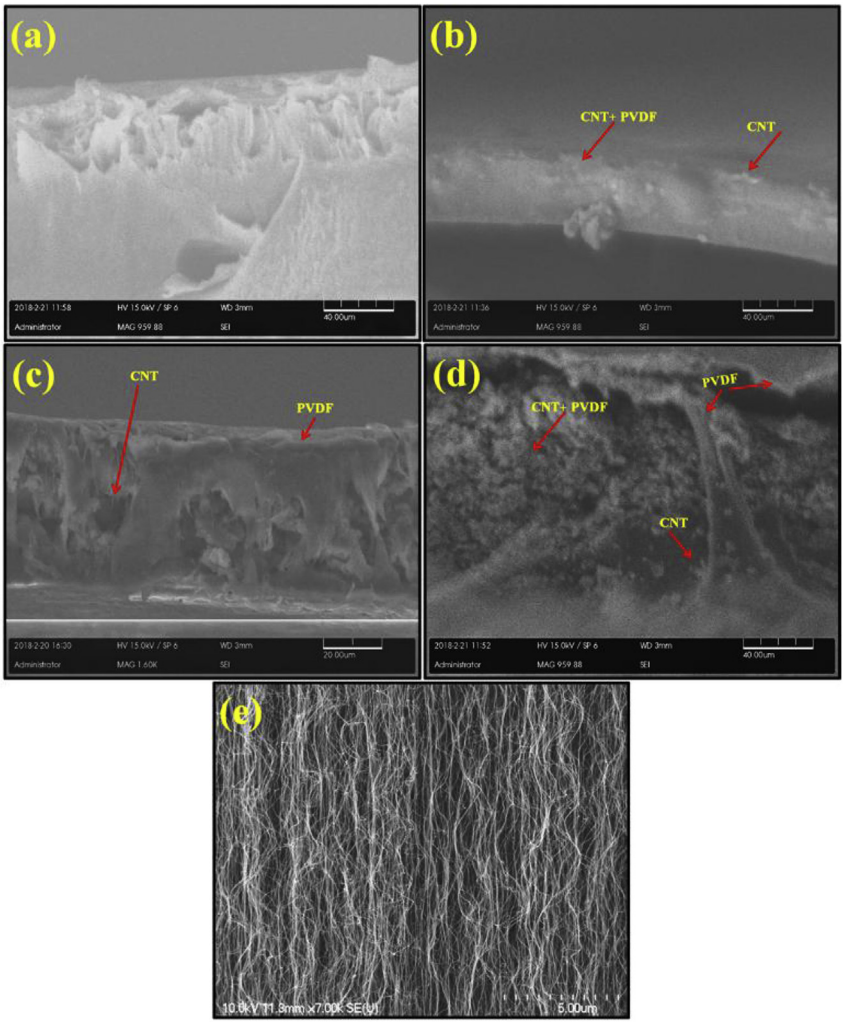

Fig. 4. SEM images of the thickness of PVDF-CNT composites films (a) pure PVDF film surface; (b) PVDF 10% with CNT; (c) PVDF 15% with CNT; (d) PVDF 20% with CNT; (e) As prepared in-house synthesized CNT forest.

obtained membrane is now thoroughly washed for several times using fresh DI water until the pH of the water and the surface of the membrane (both sides) reaches a neutral state. This is done by mildly pressing and contacting the pH paper strips to the membrane sides. After the pH is found to be at neutral point, the membranes are cleaned, dried and stored in a desiccator for further use. Table .1 shows the recipe for synthesis of PVDF-CNT composite membrane.

3. Results and discussion

3.1. Scanning electron microscope (SEM)

Scanning electron microscopes (PEMTRON PS250) and FE-SEM/EDS MIRA3 LMH TESCAN equipped with energy dispersive spectrometer (EDS) analyzer was utilized for viewing the surface topology. The images were obtained at an acceleration voltage of 15 keV using a secondary electron detector. The samples were gold coated using an ion sputter before conducting the analysis. SEM was obtained to know the morphology and thickness of the fabricated PVDF-CNT composite films. Fig. 4 represents the SEM images obtained for the films. Fig. 4 (a) shows the top surface of the TIPS induced drying of pure PVDF film. The film in general is smooth ("skin type") and translucent in nature. The surface roughness also makes the film seem porous and have good hydrophilicity. The film is almost 60 μm in thickness with similar openings across its surface. The surface at some areas shows nodular (Supplementary Fig S.1) structures formed due to the heating (drying) process. The EDX spectrum shows predominant fluorine peaks without any inclusions of another element, owing to the purity of its formula respectively. Fig. 4 (b) represents PVDF 10% with CNT, the film is around 40–45 μm thick across its length. As we can observe that the PVDF has coated the CNTs completely with traces of CNT visible across its top and bottom borders. The surface is smooth ("skin type") and also quite uniform. From the (Supplementary Fig S.2), one can also observe that the top surface is "skin type" with milder degree in roughness. Whereas, the sides (as has been cut by scissors) display a complete reinforced type structure. Upon close examination, one can observe the severed CNT forest fibers across the top and bottom layer of the composite with downward finger like flaky projections of PVDF. The elemental profile shows increased carbon content with decreasing fluoride, owing to the presence of more concentration of PVDF and also presence of CNTs. The presence of Si peak denotes few particles from the wafer when the composite was peeled off. The presence of Si and O2 peaks also infer the CNT presence. Fig. 4 (c) displays PVDF 15% with CNTs. The image shows the partial and uneven covering of the PVDF on CNTs at one point of the film edge. The total thickness of this film is 54 μm. Traces of CNTs can be observed in between the voids, topologically the surface of the film is even with random and small distribution of depression like feature. From the (Supplementary Fig S.3), one can observe that the top surface is highly uneven though "skin type" with milder roughness and depressions. The edge scan shows almost

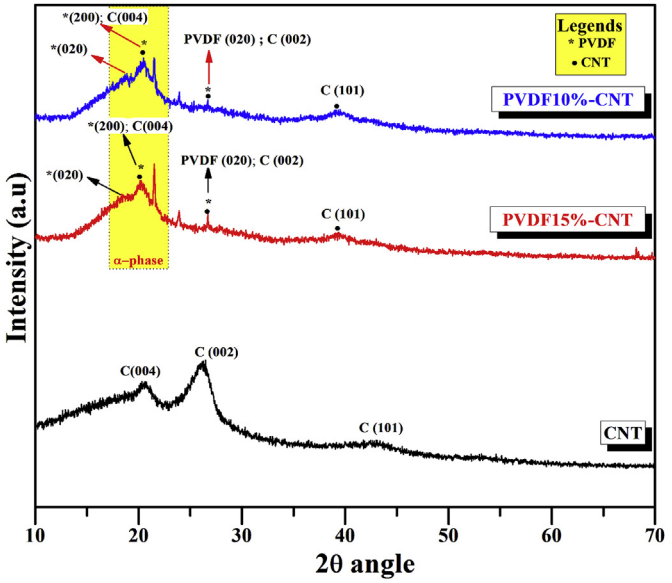

Fig. 5. X-Ray Diffractogram of CNTs and PVDF-CNT composite films.

similar results with the presence of depressions due to thin PVDF coating. As the coating density is thicker at few sides and edges, one can observe strands of CNTs standing within the thin matrix at the bottom (red circles). The elemental profile shows increasing carbon and decreasing fluorine peaks as observed in previous scans. Fig. 4 (d) displays PVDF 20% with CNTs. A similar surface distribution of PVDF is seen where the CNTs are almost covered with the PVDF but formation of double layer blanket like openings shows that the effect of drying due to heat is non-uniform. The base of the CNTs can be seen with small protrusions (arrow) of a group of CNTs. The thickness of the film is between 50 and 65 μm thick across its length. The variation in length is attributed to the amount of viscosity, the flow and drying time of the PVDF. As it is evident that by increasing concentration of PVDF, the viscosity increases thereby retarding the flow and spread of the PVDF over the CNTs. From the **(**Supplementary Fig S.4**),** one can observe that the top surface has a mixed topography with highly porous, several large sized openings and a mixed rough and "skin type" layer surrounding it. The pores when magnified shows cave like pattern with deep valleys. The edge scans shows few points of openings at the junction of the top layer but majority of the film seems to be well covered. At the opening one can also observe the presence of CNTs bursting out of the matrix. The elemental profile shows similar trend with more increase in carbon and decrease in the fluorine content as discussed above. Fig. 4 (e) represents the in-house grown CNTs on the catalyzed Si wafer using CVD at 700 °C. The CNTs are approximately 50 μm thick. The CNT forest is highly interconnected and is supported well with openings across their lengths which help in allowing an easy passage of PVDF solution during the coating and film fabrication process.

3.2. Electrostatic force microscopy (EFM)

Park systems NX-10 Atomic Force Microscopy (AFM) was employed to study the surface charge of the membranes. The instrument is equipped with the electrostatic station. A non-contact mode was employed to study the surface characteristics of the membranes. A 10 μm × 10 μm area was considered. **(**Supplementary Fig S.5**)**, shows the EFM images of the composite surface for pure PVDF, PVDF 15% with CNTs, PVDF 20% with CNTs respectively. The scan shows that the surfaces of the samples are highly rough in nature. The amplitude scales beside the image shows that the material consists of very low surface charge potential, which majorly lies in the range of 0.1–0.5 mV. The Root mean square value of roughness (R_q) in pure PVDF is around 0.217 μm with an arithmetic average height (R_a) of 0.160 μm. The (R_{pv}) peak-to-valley is around 2.756 μm respectively. For PVDF 15 %−CNT the R_q, R_a and the R_{pv} are 0.194 μm, 0.150 μm and 2.612 μm respectively. For PVDF 20 %−CNT the R_q, R_a and the R_{pv} are 0.235 μm, 0.175 μm and 2.77 μm respectively.

3.3. Focused ion beam (FIB)/transmission electron microscopy (TEM)

Higher resolution TEM (300 kV FE-TEM (Tecnai F30 S-Twin) images of the sample PVDF 10% with CNT is opted due to its thin layer of PVDF over the CNT forest. Supplementary Fig S6 shows the cross section of the composite membrane made by Dual Beam: focused ion beam (FIB) system (Helios NanoLab™). The FIB-TEM Fig S6 (a) image shows the presence of multiple dark circular components of the CNT walls within the matrix. Fig S6 (c) image shows the 5 μm thin slice with an overall cross sectional view of the composite. From the cut out, we can observe the PVDF matrix as shown by the arrows and the CNT as circular dots at the center. The top red box in the triangular zone is highlighted, magnified and displayed in Fig S6 (a) section which shows a high density of CNTs. The below marked red box is displayed in Fig S6 (d) which shows the freely spaced CNTs as observed from the top view. Fig S6 (b) shows an isolated CNT taken from the as synthesized VACNT forest respectively. The image shows that the tubes are made of 5–10 layers of graphene walls along with some amorphous carbon and few defects within the surface regions only.

Furthermore, Supplementary Fig S7 (a-e) shows the higher resolution images of the CNTs within the matrix. The yellow box displays the zone of selection for higher magnification. All the images show that the CNT walls are composed of nearly 8–10 layers respectively.

3.4. XRD

X-Ray diffraction was carried out using Bruker-Axis D8 Advance diffractometer using Cu K-alpha radiation at power of 40 mA and 40 kV respectively. The diffractograms of the samples are shown in Fig. 5. The sample shows that CNT is hetero-crystalline in nature with presence of three prominent peaks at 2(θ) theta angles with their *hkl* lattice orientations 2θ = 20.4°(004), 26.4° (002) and 42.8° (101) respectively [22,23]. The peak at 20.4° corresponds to the presence of amorphous impurities along with peak broadening at 26° for defective carbon nanotubes, thus inferring presence of semi-crystalline hexagonal graphitic planes with possible defects [24]. The peaks observed are in complete agreement with the JCPDS card #75–1621, #48–1206 and # 89–8487 respectively. The other peaks in the image **(**Fig. 5**)** represent the PVDF-CNT diffractograms. The peaks are almost similar with each other except the intensity seems to be variable. The diffraction peaks observed at 2θ angles are characteristic to PVDF viz: 18.3°, 20.5°, and 26.7° corresponds to the *hkl* orientation plane of (020), (200) and (020) which matches well with the JCPDS card # 42–1650 and # 42–1649) respectively [25–27]. The *hkl* reflection in the sample represents and confirms that the major phase of PVDF in our sample is of α-type. Also the same is observed in the FTIR results **(**Fig. 6**)** which are in agreement with each other.

3.5. FTIR

Fourier transformed Infrared spectra were obtained using Thermoscientific, (Nicolet 380) spectrometer. Fig. 6 shows the spectrum range characteristic to PVDF and CNT signature zones. From the image, peaks in between 450 and 980 cm^{-1} represents the presence of both α (major) and β-phases (minor) of PVDF. The peaks observed in between 850 and 900 cm^{-1} is attributed to the- β phase whereas remaining represents the α-phase respectively [28,29]. After introducing CNTs into the PVDF the FTIR signal changes a bit which includes a minor decrease in the intensity and change of positions for the wavenumbers between 700

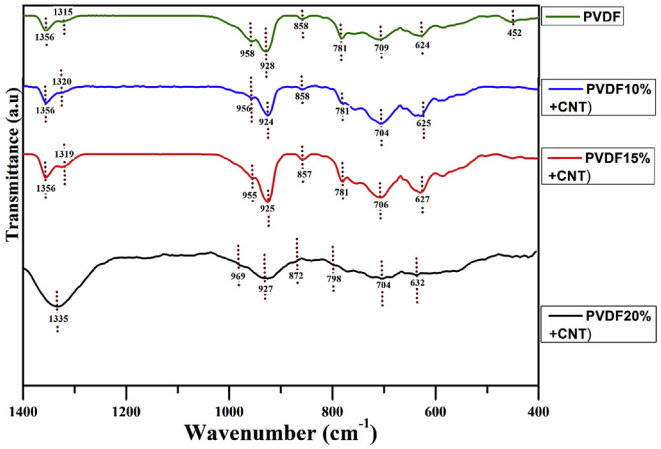

Fig. 6. FTIR spectrums of pure PVDF and PVDF-CNT composite films.

and 860 cm^{-1} respectively [30]. Secondly, the respective signature vibrations of PVDF and CNTs are visible which corresponds to the C—F (850-875 cm^{-1}) and C—N (1300-1400 cm^{-1}) stretching modes [28–30]. Since CNTs were very less in their concentration with respect to PVDF during the coating process, the signals of C—C, C—O and C—H are either very weak or not visible. The possibilities may be due to the thick PVDF coating and less concentration of CNTs [31].

3.6. Raman

Raman analysis of the samples were carried out using a microRaman spectrometer (Ramboss 500i, Dongwoo Optron Co) with an Ar^{+} ion laser source having an excitation wavelength of 514 nm. Fig. 7 shows the Raman spectrums of CNT, PVDF membrane and PVDF-CNT composite respectively. The spectrums of PVDF and PVDF-CNT composite have been selectively taken between 200-800 and 1000-1800 cm^{-1} respectively. All the PVDF-CNT composites have exhibited similar results hence only one sample spectrum has been shown in Fig. 7(d) and (e) with profile fitting using a Gauss curve. Fig. 7(a) displays the complete spectrum of the as prepared in-house CVD synthesized CNTs with a D, G and 2D (G′) bands at 1330, 1575 and 2668 cm^{-1} respectively. The I_D/I_G and $I_{G'}/I_G$ ratios 0.92 and 0.87 respectively show that the material is a heavily stacked multi-walled CNTs with several interior graphene walls. The intensity of D and G bands also show that the quality of the CNTs produced is of good quality but has few defects associated within, the secondary possibility of the increasing D band may also account for the presence of amorphous state or degenerated graphene walls as observed in the XRD at 2 theta angle of 20.4°(004), with broadening which is in agreement with the Raman results. The 2D (G′) band is observed to be almost of the same size of D band hence inferring the presence of several stacked semi degenerative graphene walls in CNTs [32,33].

The characteristic Raman spectrum of pure PVDF film is shown in Fig. 7(b) and c respectively. In Fig. 7(b) and C, the spectrum shows several α (255-658 cm^{-1}) and β-phase (1425 cm^{-1}) peaks characteristic to the PVDF [34,35]. These modes are generally from CF2-bending and CH2-rocking vibrations. Though the complete scan post 700 cm^{-1} did not yield any significant peaks except at 1425 cm^{-1} deriving that the sample is indeed made majorly of α-phase and very less of β-phase respectively [33]. This result is in complete agreement with the FTIR data. Fig. 7(d) and (e) represents the spectrums obtained for PVDF-CNT composites. All the sample spectrums show similar results. The peaks in Fig. 7(d) shows, that the α-phased peaks have shifted to lower wavelengths and baseline has also decreased after the addition of CNTs. Similarly peaks between 1300 and 1530 cm^{-1} in Fig. 7(e) is found to also change with respect to pure CNT and PVDF peak points, as we can see that the peaks: from 1330 have shifted to 1332 cm^{-1} for D-band, from 1425 to 1428 cm^{-1} for PVDF β-phase and decrease in peak position from 1575 to 1528 cm^{-1} for the G-band respectively. This implies the formation of bonds between PVDF and CNTs by charge transfer process [36,37]. As it is also observed that, the I_D/I_G ratios have increased from 0.92 for pure CNTs, to 1.08 for PVDF-CNT composite membrane amounting to the addition of C—C bonding between PVDF and CNTs through a chemical interaction by donor-acceptance at the interface [38]. According to Mohan Raja et al. [39], the increase in the ratios is also due to the increase in hydrogen bonded interaction between PVDF and CNTs, which also leads to strong adhesive and interfacial interaction properties. This assumption is in complete agreement as the membrane had strong binding force with CNTs during the pulling process. A Gaussian profile fit of the composite peak between 1300 and 1600 cm^{-1} confirms the presence of three distinct peaks as observed in Fig. 7(e) which are almost the same wavelength as observed with the original composite peak, even the I_D/I_G ratios are almost same (1.08 and 1.079 respectively). Apart from this the broadening of the composite peak between 1300 and 1530 cm^{-1} implies that the bonding between the PVDF and the surface of CNTs have taken up strongly. As the intensity at 1528 cm^{-1} has decreased, it implies to the presence of the PVDF's masking effect suggesting that the CNTs are well covered with PVDF. However, no 2D peak was observed in the composite sample scans.

3.7. Thermal analysis

Thermal analysis and stability of the samples were carried out using a Perkin Elmer STA-6000 thermogravimetric analyzer (TGA) with a heating rate of 10 °C min^{-1} in the presence of nitrogen at a flow rate of 20 ml/min. The analytical temperature range was set between room temperature and 700 °C. Fig. 8 shows the thermograms related to PVDF and PVDF-CNT composites. As the results show that all the samples have almost similar thermal trend with good thermal stability. Pure PVDF film thermogram (black line) shows temperature stability up to 450 °C. The initial loss around 135 °C is attributed to the loss of moisture along with the decomposition of polymeric fluoride (C—F) chain and residual solvent (NMP) respectively [28]. Later as the temperature progresses, at 503 °C a loss of almost 62% is recorded which is attributed to the breakdown of the polymer backbone and decomposition of the 80% of PVDF. The PVDF + CNT composites (red = PVDF 10%); (blue = PVDF 15%) and (orange = PVDF20%) shows similar trend. A small dip or loss of mass is observed at the initial point around 150 °C owing to the removal of residual solvents, breakdown of C—H and absorbed moisture as stated above, secondly a gradual mass loss up to 80–85% is recorded which is due to the evolution of HF gas as a final resultant of PVDF degradation along with the degradation of C—C bonds and C—F bonds of the PVDF and CNTs respectively [40]. A minor temperature difference is observed for the composite samples during complete degradation post 500 °C. These shifts in temperature may be due to the phase change (α-β transition) occurrence as the CNTs are also embedded within the matrix [28].

3.8. Contact angle

To investigate the membrane surface wetting property (hydrophobic/philic), a static contact angle (CA) was measured (SmartDrop Standard, FemtoFab: Korea). The constant amount of Milli-Q water (3 μl) was dispensed on the surface of the membrane and the contact angle was measured using the inbuilt software. Fig. 9 depicts the membrane contact angle as observed in real time. As it is observed the pure PVDF membrane is hydrophobic with its CA 103.6°. If we compare the SEM surface image of PVDF membrane we can observe the presence of finger like protrusion which is causing the membrane to enact the “lotus effect” [41], hence we could observe its hydrophobicity more clearly. On contrary to this, when CNT-PVDF composite is fabricated and tested for its wettability there is a decrease in the CA for all the

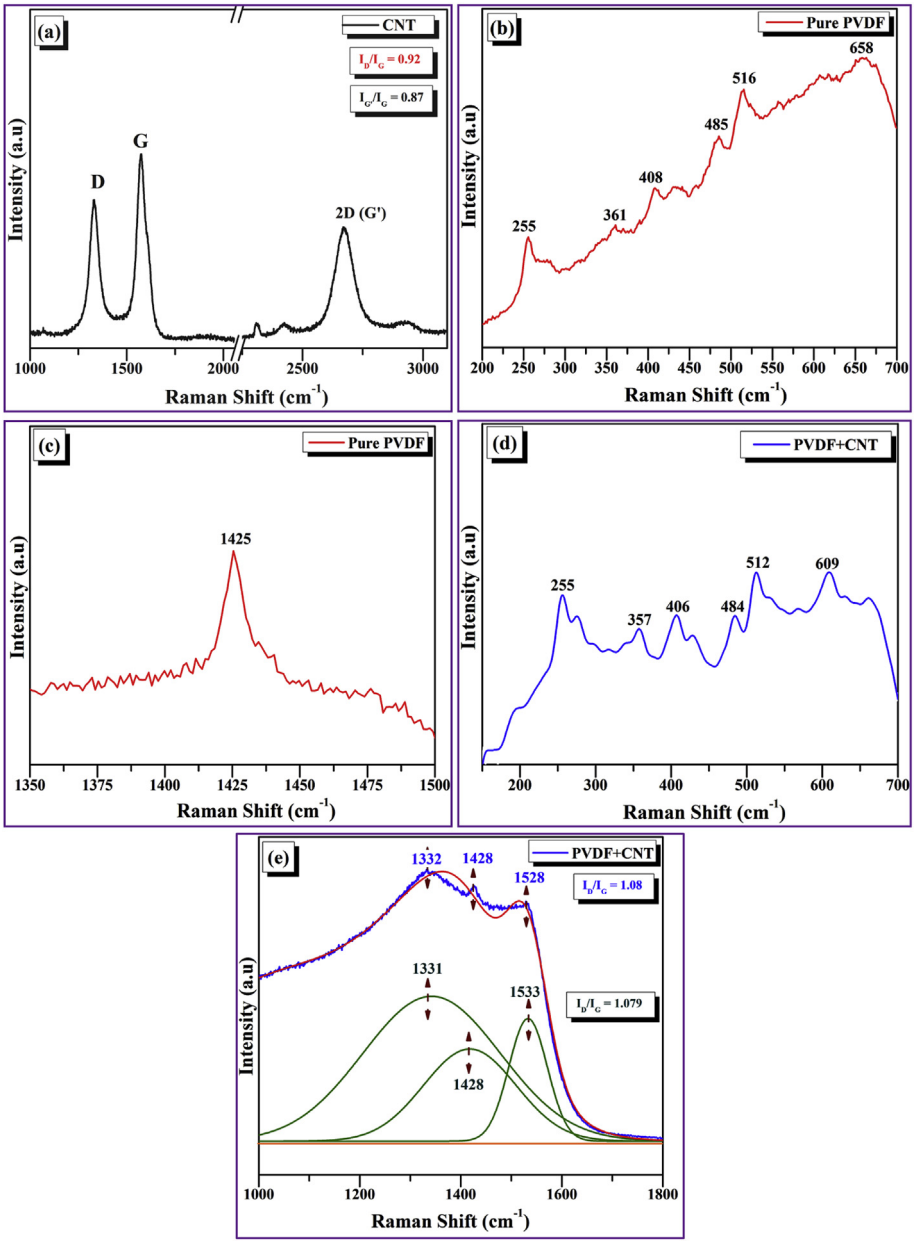

Fig. 7. Raman Spectrums of (a): the as prepared CNTs; (b), (c): Pure PVDF; and (d),(e) PVDF-CNT composite films displaying their fingerprint zone peaks.

composite samples from 89 to 87° respectively. As its a known fact that PVDF and CNTs are generally hydrophobic in nature. We believe that when the membrane is dried at 55 °C, all the solvent moieties are removed and the CNT open ends become reactive thereby creating strong bonds with the fluoride ions of PVDF resulting in the making of hydrophilic membranes. Moreover, this remarkable change may also be attributed to the development of increased surface negative charge density and the surface smoothness (skin type morphology as observed in SEM) of membrane resulting in good hydrophilicity [7].

3.9. Tensile strength

Fig. 10. Illustrates the Tensile properties of the membranes measured using a universal testing machine (Lloyd LRX Plus, Ametek Inc). The crosshead speed was 2 mm/min and the sample dimensions were 35 mm(length), 4 mm (width) with variable thickness for our samples Viz: pure PVDF = 60 μm, PVDF 10% + CNT = 40 μm, PVDF 15% + CNT = 55 μm, PVDF 20% + CNT = 65 μm respectively. Additionally, the in-house grown CNTs were also tested for its tensile property in the form of a CNT-paper. The dimension of the CNT-paper is 35 mm (length), 4 mm (width) and 35 μm (thickness). As observed from the image (Fig. 10(a)), our CNT paper can withstand stress up to 13.1 MPa with percent elongation at break appearing at 4.3% which shows a good mechanical flexibility in case of CNT. The modulus of the paper was found to be 0.25 GPa. Similar reports on CNT papers have also been reported by several authors [42–44]. Pure PVDF (Fig. 10(b)) displayed a good flexibility where it was able to withstand elongation at break up till 77% displaying its strong inter bonding between the monomers due to controlled thermal drying. Secondly, the maximum yield stress our membrane could withstand was until 54 MPa. The modulus for pure PVDF was found to be 4.2 GPa. The Composite membranes are illustrated from Fig. 10(c–e) respectively. The increasing bonding strength within the PVDF and CNTs have synergistically provided enhancement in the mechanical properties of the membranes.

As it is found when the concentration of PVDF is increased (10%,

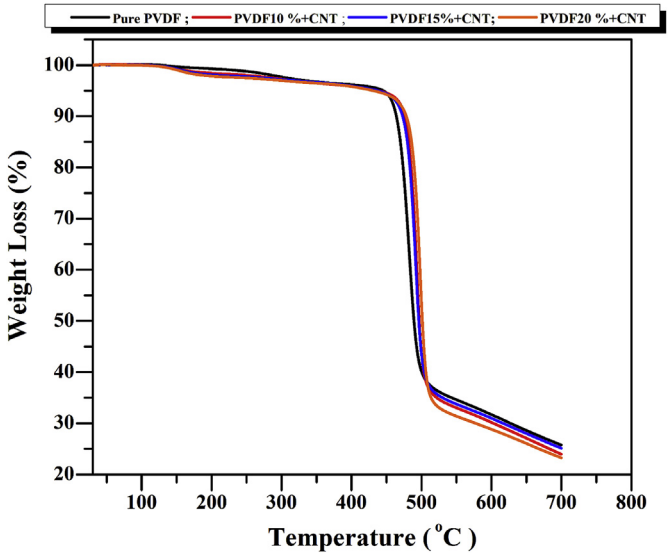

Fig. 8. Thermogravimetric data curves of Pure PVDF (Black line); PVDF10% + CNT (RedLine); PVDF15% + CNT (Blue Line); PVDF20% + CNT (Orange Line). (For interpretation of the references to colour in this figure legend, the reader is referred to the Web version of this article.)

15% and 20%), the capacity to stand higher stress improves (91%, 93% and 97%) for the samples respectively. But when elongation at break is considered, the 10 and 15% show a good increase in the elongation from 4.9% to 23.6% respectively. But as the concentration of PVDF reaches 20% the elongation at break decreases by almost half and reaches to 9.8%. We opine that, this decrease in the elongation may be attributed to the presence of micro air bubble formation and reformations in the open cell structure in microstructural networking during the drying (TIPS) process leading to possibly form weak bonds between the CNT and PVDF interface at certain areas of the membranes, and increased stiffness, which have resulted in the breakage of the sample [45–47]. The modulus of the composite samples also shows similar trend (PVDF 10% + CNT) 1.5 GPa, (PVDF 15% + CNT) 4.7 GPa and 3.5 GPa for PVDF 20% + CNT respectively.

4. Application

4.1. Filtration efficiency

PVDF-CNT composite membrane permeability tests were carried out as reported by Shawky et al. [48]. Initially the test was carried out for assessing the passage of milli-Q deionized water through the flat sheet membranes at 27 °C. The permeate volume was taken at 5min interval for 1 h at a single pressure of 1bar using a Sterlitech™ HP4750 (Sterlitech, USA) high-pressure stirred cells equipped with a dead end under stirred conditions of 800 rpm at 27 °C. The permeability was calculated as a specific flux in L/h m^2 bar units. Once the cell and the membranes were conditioned, the membrane efficiency with respect to the salt rejection was carried out. The following equations (1)–(3) were used to determine the parameters [49].

The salt rejection, R (%), was calculated by the following equation (1)

$$R(\%) = \left(\frac{Cf - Cp}{Cf}\right)x100 \quad (1)$$

Where C_f is conductivity of the feed (NaCl) solution and C_p is conductivity of the permeate solution.

The membrane flux was calculated by the following equation (2), where the flux, F (L h^{-1} m^{-2}), is defined as the volume of water "V" in

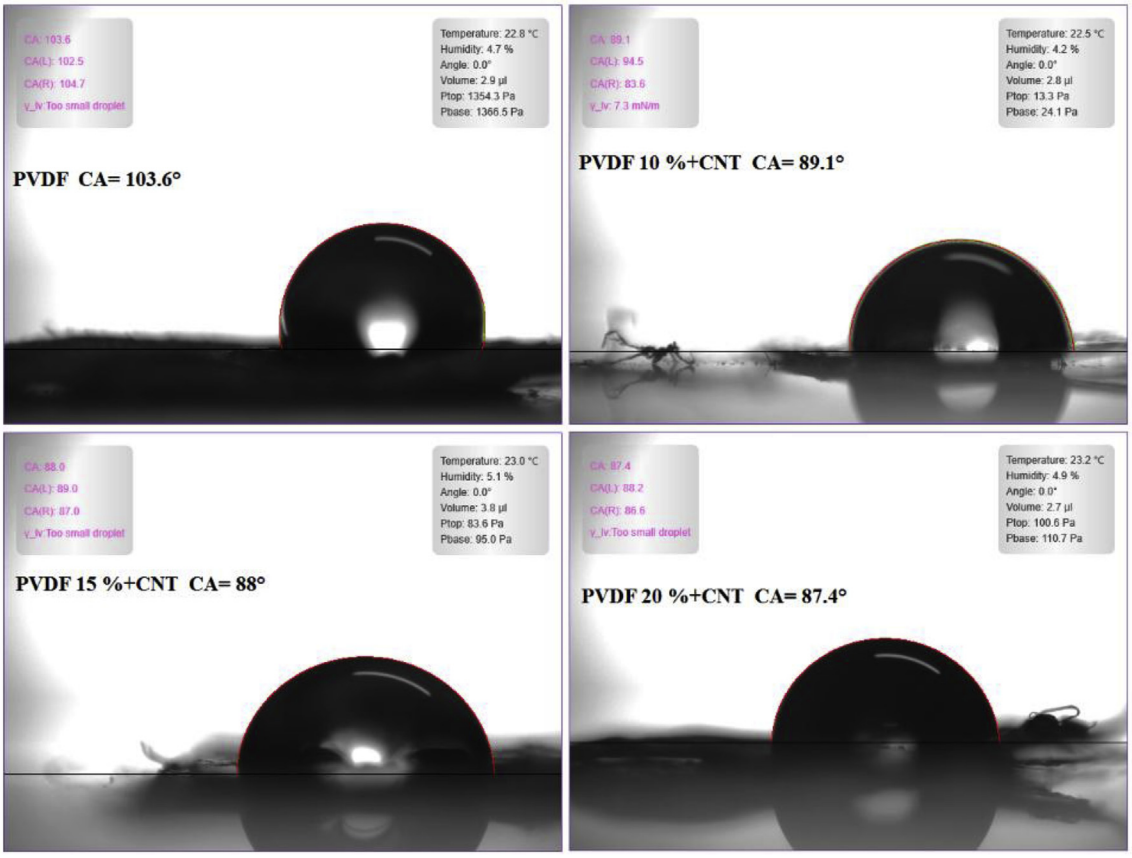

Fig. 9. Contact angle measurements of the PVDF and PVDF-CNT composite films.

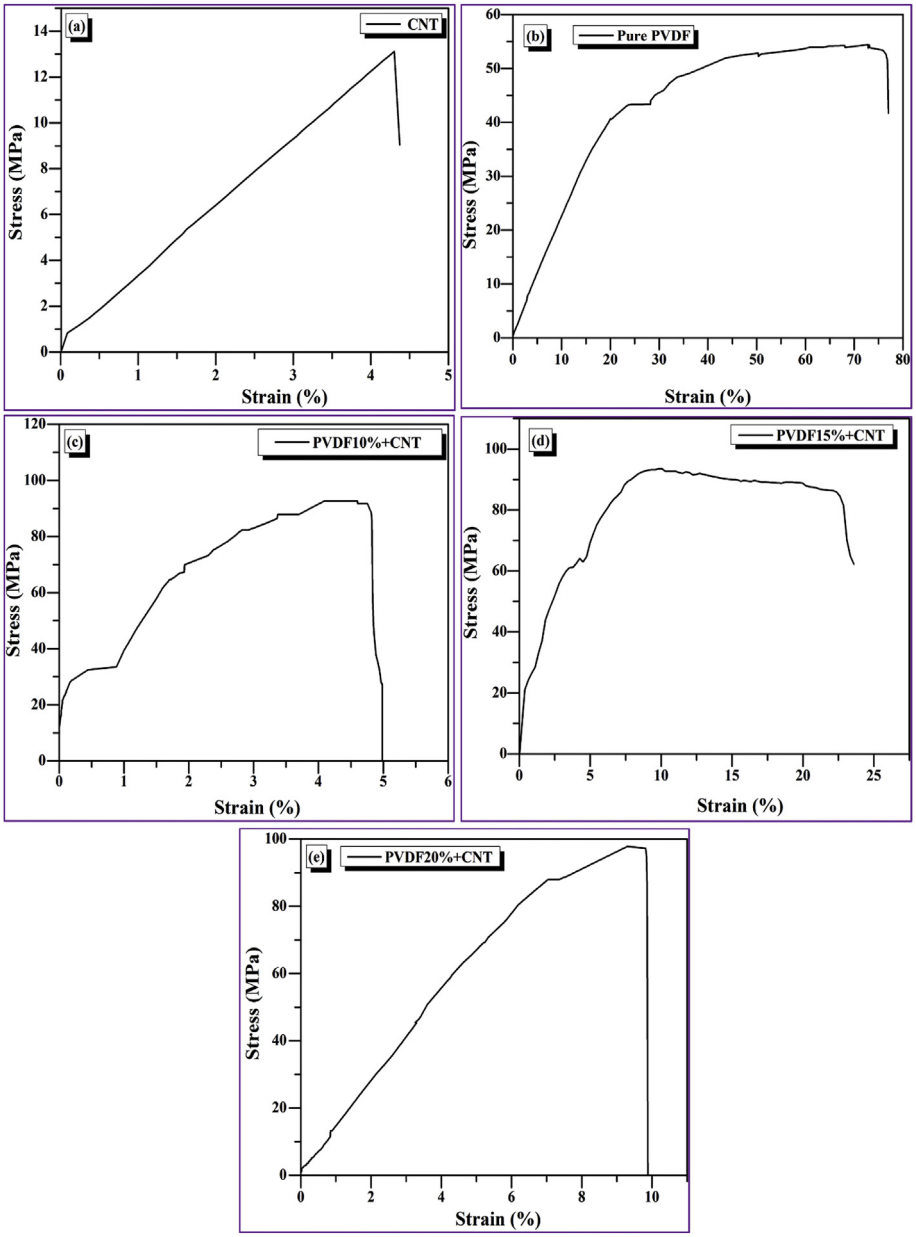

Fig. 10. Tensile test: Stress Vs Strain curves of (a): in-house grown as-prepared CNTs; (b): Pure PVDF film; (c): PVDF 10% with CNT; (d): PVDF 15% with CNT; (e): PVDF 20% with CNT.

liters (L), which has permeated through a membrane of an area "*A*" (m^2) in a time interval, "*t*" (h):

$$F = \frac{V}{A\,t} \tag{2}$$

The membrane's water permeability was calculated by the following equation (3), Where permeability, *P* (L μm m^{-2} h^{-1} bar^{-1}), is defined as the volume of water, "*V*" in liters (L), which has permeated through a membrane of area "*A*" (m^2) with a thickness "*l*" in (μm) divided by the pressure difference, "Δ*p*" in (bar), in a time interval, "*t*" (h):

$$P = \frac{V\,l}{A t\,\Delta p} \tag{3}$$

In this present work, salt (NaCl) with 0.06M(1 L) was used to analyze the efficiency of the membranes at 27 °C respectively. Throughout the filtration process the operating pressure was kept constant at 1 bar (0.1 MPa) with continuous stirring (800 rpm). Also every membrane was tested with 50 ml of NaCl as feed. The conductivity of feed and the permeate were calculated over the time using a standardized digital Mettler Toldeo (inLab741sm) conductivity meter. All the films used in this test are less than 65 μm in thickness.

The salt rejection tests (Fig. 11) were carried out on the PVDF and PVDF-CNT composite samples, as it is observed that the increasing PVDF concentration has shown an increase in salt rejection from 19 to 35% followed by a steady maintenance of the water flux with variability in the water permeability respectively. Table .2 shows the filtration parameters of all the membranes functioning at the working pressure of 1 bar. Though, the rejection rates are well below the commercially available PVDF membranes, most of the commercial membranes [6,50] generally work above 1bar of pressure, thus making our membranes suitable for working at low pressure of only 1 bar for desalination. This not only saves energy but also may filter out larger volume of seawater for future studies. Secondly, the incorporation of VACNTs into PVDF matrix has significantly improved its efficiency with respect to the membrane thickness (which is less than 65 μm in our case). This is attributed to the presence of strong network structure with

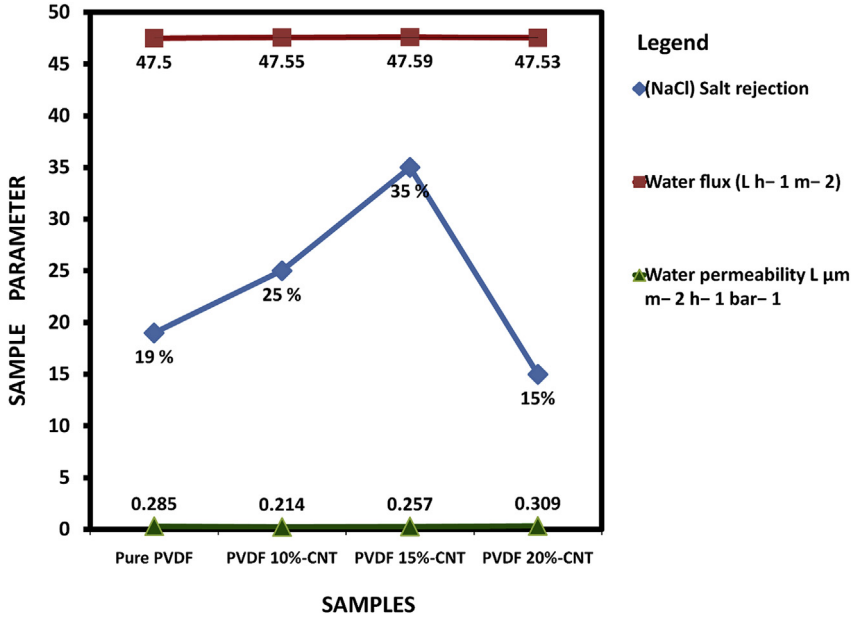

Fig. 11. Membranes salt rejection efficiencies.

fine dispersion of pores caused due to the thermal drying of the membranes [48,51–53]. In case of PVDF 15%—CNT, one can find a steady increase in the filtration efficiency due to the presence of tightly packed CNT-PVDF layer. The film shows thick layers of PVDF covering over the CNTs (as observed in SEM images). The thick layers of both CNT and PVDF may provide more salt interaction between the PVDF pores and high surface area of the CNTs leading to slightly higher filtration values. Also one can agree with the XRD image which shows that PVDF15% —CNT has high intensity of crystalline CNTs within the matrix which owes to its reactivity in salt removal respectively [48,52]. In case of PVDF20%—CNT, the trend should have increased with respect to the increasing concentration of PVDF. But it wasn't the case the authors find. In this case when the sample was examined by SEM we found that the surface of the membrane was having mixed topology with very large distribution of pores with size greater than 8–10 µm. This must have caused limited interaction of the salt solution with the matrix and CNT surface charge. Hence seepage of the feed must have been easier there by decreasing the filtration efficiency. Baskoro et al. stated that rejected molecule tends to get built up in concentrated form around the boundary layer contiguous to the membrane surface [54,55]. This reduces the dynamic force for filtration. Recently Xu et al. reported that the inter-lamellar structure of the membrane can effectively control the permeate's transport [56]. When the feed concentration is high, the Na^+ ions interact with the functional arms of the CNTs (COO^-), within the membrane there by leading to a reduced Donnan exclusion effect. This reduced interaction results in the low salt rejection [54]. One can also compare that, most of the commercially available membranes are at least 50–200 µm in thickness when compared to our membranes which are less than 65 µm respectively, which are 3.5 times thinner than the commercial ones. Moreover, the mechanical strength of our very thin membranes is also high with respect to withstanding the maximum operating pressure up to 90 ± 5 MPa (900 ± 50 bar) which according to us is the lowest reported thickness based pressure sustenance for PVDF-CNT membranes. Authors to the best of their knowledge related to VACNT-polymer based membranes have tabulated and compared their work based on the thickness of the film, its chemical composite makeup and the working pressure along with its rejection efficiency in Supplementary Table.S1. Our future study would be oriented to enhance the salt rejection efficiency of the very thin membranes by employing surface changes and doping techniques so that the flux and permeate also normalizes simultaneously.

4.2. Effect of PVDF concentration on morphology and filtration

As a binary system, TIPS process generally involves the use of a polymer and a solvent for defect free manufacture of composites. Hence this process offers higher reproducibility with very low defects. Thus, TIPS process yields in the fabrication of defect free, robust membranes with improved mechanical strength in the presence of high concentrated polymers. This is due to the fact that higher temperatures allow for better and excellent crystallization. TIPS process offers several advantages like prefabrication of micro-porous membrane composites with narrow pore size distribution, unique morphology and high porosity [57–59] based on the composition and temperature respectively. This process faces a major challenge to be addressed in controlling the pore size (> 50 nm) based on the utilization of excessive temperature for membrane fabrication. During the quenching process, using water when the membrane is formed a mild non-solvent induced phase separation (NIPS) effect takes place on the surface which results in the formation of dense “Skin like” topology [58]. Moreover in our case we find several points of agreement with the effect of increasing concentration of PVDF (from 5 to 20 w/w %) (please refer Table .1) with

Table 2
Salt rejection efficiency of PVDF and PVDF-CNT Membranes.

Membrane Name	Feed pressure (bar)	Water flux ($L\,h^{-1}\,m^{-2}$)	Water permeability ($L\,\mu m\,m^{-2}\,h^{-1}\,bar^{-1}$)	(NaCl) Salt rejection (%)
Pure PVDF	1	47.50	0.285	19%
PVDF 10%—CNT	1	47.55	0.214	25%
PVDF 15%—CNT	1	47.59	0.257	35%
PVDF 20%—CNT	1	47.53	0.309	15%

Note: Feed concentration: 35 g/L (0.06M NaCl) and feed test volume/membrane: 50 ml.

respect to constant amount of NMP as the dope solvent. As observed correlatively with SEM, XRD, tensile and other characterization tools employed in our case, we find that the membranes have "skin like" morphology and with increasing polymer content, surface openings in the form of "cave like patterned holes" are observed. Indicating the effect of temperature and rapid evaporation of the solvent. Higher the polymer content till the threshold limit, offers very good mechanical properties. Beyond this, the material tends to show brittle nature due to immiscibility and formation of bigger disentangled spherulites [58]. Hydrophilicity of the membranes also improved with the increasing amount of polymer. The contact angle values have come down from 103° to 87° respectively. This infers that the increasing concentration of the PVDF does have effect in improving the morphology, filtration efficiency, hydrophilicity and mechanical properties respectively.

5. Conclusion

A facile approach to the fabrication of ultrathin and light weight PVDF-CNT composite was designed by TIPS method. Additionally, the VACNTs were synthesized on a Si substrate using a thermal CVD. PVDF in different aliquots were synthesized and a very small volume was poured on to the VACNTs to cover them and form freestanding membranes after drying and acid digestion. The Pure PVDF and PVDF-CNT composites were found to be hydrophilic and thermally stable with enhanced mechanical stability and durability. The membranes had a medium thickness in the range of 30–60 μm which were assessed for their salt rejection efficiency at 1 bar of working pressure. The membranes could efficiently remove 0.06 M NaCl up to 35%, with similar water flux and almost very less energy. The mechanical stability of the membranes was found to be very good with respect to its modulus and strain relations, as most of the membranes were able to withstand high pressures also. The effect of increasing concentration of PVDF from 5 to 20 w/w% shows considerable changes and improvement in the morphology, mechanical property, water filtration efficiency and hydrophilicity of the membranes. In our future work this will help us to explore further diverse applications in the field of industrial and domestic pollution related treatment processes. We also focus our next study on membranes to be reusable, as we know that PVDF is mostly inert and non-reactive to acid-base reactions making it more meritorious for several cycles of reuse without any damage to it.

Acknowledgement

This study was financially supported by the "2017 Post-Doc. Development Program" of Pusan National University, and supported by Basic Science Research Program through the National Research Foundation of Korea (NRF) funded by the Ministry of Education (2015R1D1A3A01019420). Also, this research was partially supported by Creative Materials Discovery Program through the National Research Foundation of Korea (NRF) funded by Ministry of Science and ICT, South Korea (NRF-2017M3D1A1039287). The author (VD) would like to thank the Pusan National University, Busan, Korea for supporting the post-doctoral fellowship and funding the current project.

Appendix A. Supplementary data

Supplementary data to this article can be found online at https://doi.org/10.1016/j.compositesb.2018.12.106.

References

[1] Kang GD, Cao YM. Application and modification of poly(vinylidene fluoride) (PVDF) membranes -A review. J Membr Sci 2014;463:145–65.
[2] Rajabzadeh S, Maruyama T, Ohmukai Y, Sotani T, Matsuyama H. Preparation of PVDF/PMMA blend hollow fiber membrane via thermally induced phase separation (TIPS) method. Separ Purif Technol 2009;66:76–83.
[3] Jiang J, Zhu L, Zhu L, Zhu B, Xu Y. Surface characteristics of a self-polymerized dopamine coating deposited on hydrophobic polymer films. Langmuir 2011;27:14180–7.
[4] Zhang W, Shi Z, Zhang F, Liu X, Jin J, Jiang L. Superhydrophobic and superoleophilic PVDF membranes for effective separation of water-in-oil emulsions with high flux. Adv Mater 2013;25:2071–6.
[5] Liu F, Hashim A, Liu Y, Abed MRM, Li K. Progress in the production and modification of PVDF membranes. J Membr Sci 2011;375:1–27.
[6] Ji J, Liu F, Hashim NA, Abed MRM, Li K. Poly(vinylidene fluoride) (PVDF) membranes for fluid separation. React Funct Polym 2015;86:134–53.
[7] Rana D, Matsuura T. Surface modifications for antifouling membranes. Chem Rev 2010;110:2448–71.
[8] Kang GD, Cao YM. Development of antifouling reverse osmosis membranes for water treatment: a review. Water Res 2012;46:584–600.
[9] Huang W, Li Z, Chen X, Tian P, Wang X. Pressure-controlled growth of piezoelectric low-dimensional structures in ternary fullerene C60/carbon nanotube/poly (vinylidene fluoride) based hybrid composites. Compos B Eng 2014;62:126–36.
[10] Salavati-Niasari M, Davar F, Bazarganipour M. Synthesis. characterization and catalytic oxidation of para-xylene by a manganese(III) Schiff base complex on functionalized multi-wall carbon nanotubes (MWNTs). Dalton Trans 2010;39:7330–7.
[11] Salavati-Niasari M, Bazarganipour M. Covalent functionalization of multi-wall carbon nanotubes (MWNTs) by nickel(II) Schiff-base complex: synthesis, characterization and liquid phase oxidation of phenol with hydrogen peroxide. Appl Surf Sci 2008;255:2963–70.
[12] Zhang DP, Tian PF, Chen X, Lu J, Zhou ZW, Fan XM, et al. Fullerene C60-induced growth of hollow piezoelectric nanowire arrays of poly (vinylidene fluoride) at high pressure. Compos Sci Technol 2013;77:29–36.
[13] Salavati-Niasari M, Bazarganipour M. Synthesis, characterization and catalytic oxidation properties of multi-wall carbon nanotubes with a covalently attached copper (II) salen complex. Appl Surf Sci 2009;255:7610–7.
[14] Salavati-Niasari M, Esmaeili E, Seyghalkar H, Bazarganipour M. Cobalt(II) Schiff base complex on multi-wall carbon nanotubes (MWNTs) by covalently grafted method: synthesis, characterization and liquid phase epoxidation of cyclohexene by air. Inorg Chim Acta 2011;375:11–9.
[15] Wang S, Liang S, Liang P, Zhang XY, Xia Huang. In-situ combined dual-layer CNT/PVDF membrane for electrically-enhanced fouling resistance. J Membr Sci 2015;491:37–44.
[16] Hong SK, Lee HW. The effect of diffusion barrier and thin film deposition temperature on change of carbon nanotubes length. J Korean Powder Metall Inst 2017;24(3):248–53.
[17] Terrado E, Redrado M, Munoz E, Maser WK, Benito AM, Martinez MT. Aligned carbon nanotubes grown on alumina and quartz substrates by a simple thermal CVD process. Diam Relat Mater 2006;5:1059–63.
[18] Hayashi Y, Iijima T, Miyake M, Satoh M, Tanmemura M. Growth evolution of rapid grown aligned carbon nanotube forests without water vapor on Fe/Al2O3/SiO2/Si substrate. Diam Relat Mater 2011;20(7):859–62.
[19] Suvac E, Çelik Y, Weibel A, Peigney A, Flahaut E. Organized growth of carbon nanotubes on Fe-doped alumina ceramic substrates. Carbon 2012;50(8):3092–5.
[20] Jeong DW, Shin UH, Kim JH, Kim SH, Lee HW, Kim JM. Stable hierarchical superhydrophobic surfaces based on vertically aligned carbon nanotube forests modified with conformal silicone coating. Carbon 2014;79:442–9.
[21] Mathur A, Wadhwa S, Tweedie M, Hazra KS, Dickinson C, Roy SS, Mitra SK, Misra DS, McLaughlin JA. A comparative study of the growth, microstructural and electrical properties of multiwall CNTs grown by thermal and microwave plasma enhanced CVD methods. Physica E Low Dimens Syst Nanostruct 2011;44(1):29–36.
[22] Arulmani S, Wu JJ, Anandan S. Amphiphilic Triblock Copolymer guided Polyaniline embraced CNT nanohybrid with outcropping whiskers as an energy storage electrode. Electrochim Acta 2017;246:737–47.
[23] Coqa B, Planeix JM, Brotons V. Fullerene-based materials as new support media in heterogeneous catalysis by metals. Appl Catal Gen 1998;173(2):175–83.
[24] Xiong H, Motchelaho MAM, Moyo M, Jewell LL, Coville NJ. Cobalt catalysts supported on a micro-coil carbon in Fischer–Tropsch synthesis: a comparison with CNTs and CNFs. Catal Today 2013;214:50–60.
[25] Davis GT, Mckinney JE, Broadhurst MQ, Roth SC. Electric-field-induced phase changes in poly(vinylidene fluoride). J Appl Phys 1978;49:4998–5002.
[26] Lin DJ, Chang HH, Chen TC, Lee YC, Cheng LP. Formation of porous poly(vinylidene fluoride) membranes with symmetric or asymmetric morphology by immersion precipitation in the water/TEP/PVDF system. Eur Polym J 2006;42:1581–94.
[27] Mapunda EC, Mamba BB, Msagati TAM. Carbon nanotube embedded PVDF membranes: effect of solvent composition on the structural morphology for membrane distillation. Phys Chem Earth 2017;100:135–42.
[28] Mishra S, Kumaran K, Sivakumaran R, Pandian SP, Kundu S. Synthesis of PVDF/CNT and their functionalized composites for studying their electrical properties to analyze their applicability in actuation & sensing. Colloids Surf, A 2016;509:684–96.
[29] Wang S, Liang S, Liang P, Zhang X, Huang X. In-situ combined dual-layer CNT/PVDF membrane for electrically-enhanced fouling resistance. J Membr Sci 2015;491:37–44.
[30] Yang JH, Xiao YJ, Yang CJ, Li ST, Wang Y. Multifunctional poly(vinylidene fluoride) nanocomposites via incorporation of ionic liquid coated carbon nanotubes. Eur Polym J 2018;98:375–83.
[31] Zhang WB, Zhang ZX, Yang JH, Huang T, Zhou ZW. Largely enhanced thermal conductivity of poly(vinylidene fluoride)/carbon nanotube composites achieved by adding graphene oxide. Carbon 2015;90:242–54.
[32] Dresselhaus MS, Dresselhaus G, Saito R, Jorio A. Raman spectroscopy of carbon nanotubes. Phys Rep 2005;409(2):47–99.

[33] Elashmawi IS, Gaabour LH. Raman, morphology and electrical behavior of nanocomposites based on PEO/PVDF with multi-walled carbon nanotubes. Respir Physiol 2015;5:105–10.
[34] Gharabli SA, Kujawa J, Mavukkandy MO, Arafat HA. Functional groups docking on PVDF membranes: novel Piranha approach. Eur Polym J 2017;96:414–28.
[35] Lang WZ, Zhang X, Shen JP, Xu HP, Xu ZL, Guo YJ. The contrastive study of chemical treatment on the properties of PVDF/PFSA and PVDF/PVP ultrafiltration membranes. Desalination 2014;341:72–82.
[36] Rao AM, Eklund PC, Bandow S, Thess A, Smalley RE. Evidence for charge transfer in doped carbon nanotube bundles from Raman scattering. Nature 1997;388:257–9.
[37] Zhang ZC, Gu YZ, Wang SK, Li QW, Li M, Zhang ZG. Enhanced dielectric and mechanical properties in chlorine-doped continuous CNT sheet reinforced sandwich polyvinylidene fluoride film. Carbon 2016;107:405–14.
[38] Yee WA, Kong J, Zhang C, Liu T, Kotaki M, Lu X. Polymorphism of electrospun polyvinylidene difluoride/carbon nanotube (CNT) nanocomposites: synergistic effects of CNT surface chemistry, extensional force and supercritical carbon dioxide treatment. Polymer 2012;53(22):5097–102.
[39] Raja M, Ryu SH, Shanmugharaj AM. Influence of surface modified multiwalled carbon nanotubes on the mechanical and electroactive shape memory properties of polyurethane (PU)/poly(vinylidene diflouride) (PVDF) composites. Colloids Surf, A 2014;450(1):59–66.
[40] Shen Y, Lua AC. Preparation and characterization of mixed matrix membranes based on poly(vinylidene fluoride) and zeolite 4A for gas separation. Polym Eng Sci 2012;52:2106–13.
[41] Choi DW, Yoo JW, Park SM, Kim DS. Facile and cost-effective fabrication of paternable superhydrophobic surfaces via salt dissolution assisted etching. Appl Surf Sci 2017;393:449–56.
[42] Li Z, Xu J, O'Byrne JP, Chen L, Wang K, Morris MA, et al. Freestanding bucky paper with high strength from multi-walled carbon nanotubes. Mater Chem Phys 2012;135:921–7.
[43] Ghamsari AK, Wicker S, Woldesenbet E. Bucky syntactic foam; multi-functional composite utilizing carbon nanotubes-ionic liquid hybrid. Compos B Eng 2014;67:1–8.
[44] Coleman JN, Blau WJ, Dalton AB, Munoz E, Collines S, Kim BG, et al. Improving the mechanical properties of single-walled carbon nanotube sheets by intercalation of polymeric adhesives. Appl Phys Lett 2003;82(11):1682–4.
[45] Kim HS, Song MS, Seo JW, Shin US. Preparation of electrically conductive buckysponge using CNT-cement: conductivity control using room temperature ionic liquids. Synth Met 2014;196:92–8.
[46] Bagotia N, Choudhary V, Sharma DK. Studies on toughened polycarbonate/multi-walled carbon nanotubes nanocomposites. Compos B Eng 2017;124:101–10.
[47] Lee HG, Kim GH, Ha CS. Polyimide/amine-functionalized cellulose nanocrystal nanocomposite films. Mat Today Commun 2017;13:275–81.
[48] Shawky HA, Chae SR, Lin SH, Wiesner MR. Synthesis and characterization of a carbon nanotube/polymer nanocomposite membrane for water treatment. Desalination 2011;272:46–50.
[49] Wang K, Zeng Y, He L, Yao J, Suresh AK, Bellare J, Sridhar T, Wang H. Evaluation of quaternary phosphonium-based polymer membranes for desalination application. Desalination 2012;292:119–23.
[50] Cui Z, Drioli E, Lee YM. Recent progress in fluoropolymers for membranes. Prog Polym Sci 2014;39:164–98.
[51] Song R, Yang D, He L. Preparation of semi-aromatic polyamide(PA)/multi-wall carbon nanotube (MWCNT) composites and its dynamic mechanical properties. J Mater Sci 2008;43:1205–13.
[52] Li W, Chen X, Chen C, Xu L, Yang Z, Wang Y. Preparation and shear properties of carbon nanotubes/poly(butyl methacrylate) hybrid material. Polym Compos 2008;29(9):972–7.
[53] Lee SY, Kim HJ, Patel R, Im SJ, Kim JH, Min BR. Silver nanoparticles immobilized on thin film composite polyamide membrane: characterization, nanofiltration, antifouling properties. Polym Adv Technol 2007;18:562–8.
[54] Baskoro F, Wong CB, Kumar SR, Chang CW, Chen CH, Chen DW, Lue SJ. Graphene oxide-cation interaction: inter-layer spacing and zeta potential changes in response to various salt solutions. J Membr Sci 2018;554:253–63.
[55] Mulder J. Basic principles of membrane technology. Springer Science & Business Media; 2012. p. 416–64.
[56] Xu WL, Fang C, Zhou F, Song Z, Liu Q, Qiao R, Yu M. Self-assembly: a facile way of forming ultrathin, high-performance graphene oxide membranes for water purification. Nano Lett 2017;17:2928–33.
[57] Kim JF, Kim JH, Lee YM, Drioli E. Thermally induced phase separation and electrospinning methods for emerging membrane applications: a review. AIChE J 2016;62:461–90.
[58] Kim JF, Jung JT, Wang HH, Lee SY, Moore T, Sanguineti A, Drioli E, Lee YM. Microporous PVDF membranes via thermally induced phase separation (TIPS) and stretching methods. J Membr Sci 2016;509:94–104.
[59] Jung JT, Wang HH, Kim JF, Lee J, Kim JS, Drioli E, Lee YM. Tailoring nonsolvent-thermally induced phase separation (N-TIPS) effect using triple spinneret to fabricate high performance PVDF hollow fiber membranes. J Membr Sci 2018;559:117–26.